Inorganic Chemistry
Cite This: Inorg. Chem. 2019, 58, 3473−3478
Article
pubs.acs.org/IC

Remote Bonding in Clusters $[Pd_3Ge_{18}R_6]^{2-}$: Modular Bonding Model for Large Clusters via Principal Interacting Orbital Analysis

Jing-Xuan Zhang, Fu Kit Sheong,* and Zhenyang Lin*

Department of Chemistry, The Hong Kong University of Science and Technology, Clear Water Bay, Kowloon, Hong Kong, People's Republic of China

Supporting Information

ABSTRACT: Main group cluster compounds have attracted increasing attention in the past decades. Despite recent developments in their synthesis, the description of their electronic structures is usually limited to simply applying Wade's rule originally developed for borane compounds. This traditional approach is once again challenged by two recently reported group 14 metalloid clusters in the form of $[Pd_3Ge_{18}R_6]^{2-}$. In this work, we put forward a modular bonding model for these two clusters, via principal interacting orbital (PIO) analysis. The site preference for six substituents has also been analyzed.

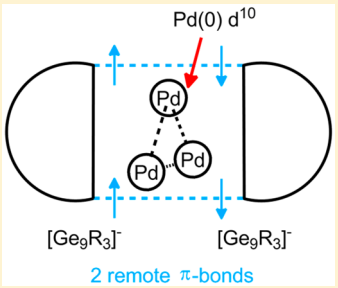

Group 14 metalloid clusters have recently attracted a lot of interest due to their distinctive structural diversity and associated fascinating chemistry.[1−5] A great number of cluster compounds have been synthesized with moieties consisting of group 14 elements during the last decades.[6−10] In particular, clusters in the form of $[E_9]^{n-}$ (E = Si, Ge, Sn, Pb; n = 2−4) are commonly observed in experiments.[11−27] Despite rapid synthetic developments, bonding models concerning electronic structures of these clusters are rather limited. In order to understand a group 14 metalloid cluster, one normally draws an analogy with a well-studied borane cluster and simply applies Wade's rule. While this approach successfully explains a number of group 14 metalloid clusters, exceptions to Wade's rule still arise from time to time.[28] Examination of such exceptions would give us a more comprehensive picture on cluster chemistry.

In this work, we are going to present our bonding study on the recently reported cluster compounds $[Pd_3Ge_{18}R_6]^{2-}$ (R = Sn^{i}Pr$_3$, (**1**); R = Si^{i}Pr$_3$, (**2**))[29,30] that serve as one more piece to this puzzle (Figure 1a,b). In order to achieve a clear understanding of the structure and bonding in these clusters, instead of constructing the whole set of molecular orbitals (MOs) and trying to comprehend the cluster in a global manner (as how Wade's rule works), we are going to adopt a (semi)localized point of view based on fragment orbital interactions by means of principal interacting orbital (PIO) analysis.[31] By dividing the whole cluster into two $[Ge_9R_3]$ moieties and a Pd_3-triangle, we found that there exists a pair of remote bonds between the two $[Ge_9R_3]$ moieties, although they are geometrically separated by the Pd_3-triangle. By comparing these compounds with other clusters which also contain Ge_9 moieties, we will show the necessity of this approach not only in helping us understand the electronic structure of these large molecules but also in explaining the experimentally observed atypical substitution pattern.[30]

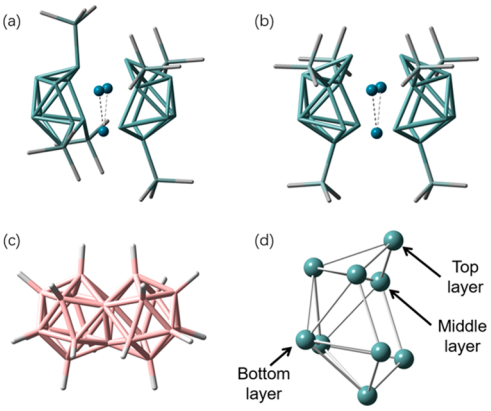

Figure 1. Optimized structures of cluster compounds (a) **1′**, (b) **2′**, and (c) $[B_{21}H_{18}]^-$ and (d) labeling scheme of Ge atoms in a Ge_9 cage.

During the past years, Sevov and co-workers have reported the syntheses of the cluster compounds **1** and **2** in *Journal of the American Chemical Society*.[29,30] Both clusters adopt a geometry of a Pd_3-triangle sandwiched by two Ge_9R_3 moieties. At first glance, a simple electron count leads to a total number of 80 (= 4 from each Ge × 18 + 6 from substituents + 2 from net charge + 0 from the three Pd(0) centers) electrons, while its 21-vertex borane analogue $[B_{21}H_{18}]^-$ (Figure 1c) has 82 (= 3 from each B × 21 + 18 from hydrogens + 1 from net charge) electrons.[32] This implies that such naive analogy with borane clusters is not sufficient to describe the electronic structures of these clusters, not to mention that the borane compound $[B_{21}H_{18}]^-$ itself does not simply follow Wade's rule and

Received: December 29, 2018
Published: February 21, 2019

DOI: 10.1021/acs.inorgchem.8b03640
Inorg. Chem. 2019, 58, 3473−3478

requires extended rules such as $(m + n + o)$ rules put forward by Jemmis and co-workers.[33,34]

Moreover, the substitution sites are different between clusters **1** and **2**. A Ge_9 cage with 3-fold symmetry can be divided into three groups of symmetry-related Ge atoms. In this paper, the three symmetry-related Ge atoms on the open face of the Ge_9 cage are labeled as the "top layer"; the next three symmetry-related Ge atoms are labeled as the "middle layer" and the remaining three as the "bottom layer" (Figure 1d). In cluster **2**, the two Ge_9 cages are both decorated (bonded) with three R substituents on the middle layer, leading to an eclipsed arrangement of the six substituents and a pseudo-D_{3h} symmetry for the whole cluster. On the other hand, the decorated sites in cluster **1** are different, leading to a staggered conformation among the six substituents and a pseudo-C_{3v} symmetry only. Such a subtle feature cannot be well explained by any electron-counting approach because each substituent would be counted as a formal one-electron donor to the whole cluster regardless of the substitution site. A clearer and more accurate description of the electronic structure of the clusters is therefore needed to answer these very fundamental questions. As the skeletal geometries are similar in both clusters **1** and **2**, we will begin our discussion with the electronic structure of cluster **1** and then proceed to cluster **2** when analyzing the site preference of substituents.

A commonly adopted modular practice to understand the electronic structure of a cluster compound is to partition it into pieces whose electronic structures are familiar to us. Hence, our first attempt is to partition the cluster into two $Ge_9R_3^-$ cages and a neutral Pd_3-triangle. $Ge_9R_3^-$ has been found to be an important building unit in a number of recently synthesized decorated zintl ions and their derivatives.[11−21] Neutral d^{10} centers are also common in a variety of cluster compounds.[20,23,25,26] The much longer Pd−Pd distances in **1** (2.88 Å in crystal and 2.92 Å in DFT optimization) than that in bulk metal also suggest no significant Pd−Pd interactions and support our neutral assignment of the Pd_3 centers. One might then take for granted that cluster **1** should be understood as two $Ge_9R_3^-$ cages coordinating to the three Pd centers, as there are other examples where $Ge_9R_3^-$ cages act as ligands.[11−14,16,17,20] However, we note that, in cluster **1**, the structures of the two $Ge_9R_3^-$ cages are different from either monocapped square antiprism as predicted by Wade's $(n + 2)$ rule for *nido* clusters or tricapped trigonal prism as observed in other crystal structures.[11−14,18−22] Hence, what interaction brings together the two Ge_9R_3 cages and the Pd_3-triangle requires further investigation.

In order to obtain a precise description of the bonding interaction in compound **1**, we performed a DFT study using the simplified model $[Pd_3Ge_{18}(SnMe_3)_6]^{2-}$ (**1′**), followed by PIO analysis. PIO analysis is a newly developed bonding analysis tool aimed at identifying the dominant orbital interactions between two selected fragments.[31] We first performed the PIO analysis on cluster **1′** with the three Pd centers being fragment A and all the rest of the atoms (two Ge_9R_3 moieties) being fragment B. The results of this PIO analysis indicate only donor−acceptor interactions are present between two Ge_9R_3 cages and the Pd_3-triangle; namely, the Pd centers donate their 4d electrons to the two Ge_9R_3 cages and meanwhile stabilize the skeletal (cage) bonding orbitals using their 5s orbitals (Figure S1). The results from the PIO analysis are consistent with our understanding that the Pd centers have d^{10} configurations and formally do not contribute electrons to the skeletal bonding. The near-zero NPA charge[35] calculated for each Pd center (0.03) also agrees with this argument.

Interestingly, another round of PIO analysis provides more valuable information on the overall electronic structure of compound **1′**, in which one Ge_9R_3 cage is taken as fragment A and the other Ge_9R_3 cage taken as fragment B. Note that these two cages differ only by substitution sites. Results show that each cage has two degenerate PIOs that dominate the interaction between two cages as shown in Figure 2a. Each

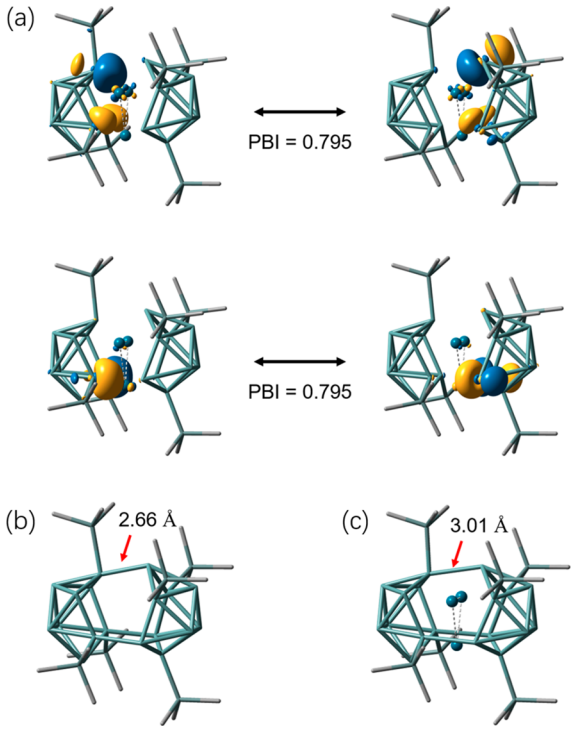

Figure 2. (a) Top two PIO pairs of compound **1′**, with the two fragments of concern being two Ge_9R_3 cages, respectively. (b) Optimized structure and selected bond lengths of the hypothetical cluster $[Ge_{18}(SnMe_3)_6]^{2-}$. (c) Optimized structure and selected bond lengths of the cluster **1′** $[Pd_3Ge_{18}(SnMe_3)_6]^{2-}$.

orbital has an occupation number close to 1 (0.96−1.18), and the PIO-based bond index (PBI) is also significant (0.795), indicating that there indeed formally exists a pair of "π-bonds" between the two Ge_9R_3 cages, which involve multiple centers, with minimal involvement of the Pd_3 centers. Actually, the two PIOs of each cage resemble to a large extent the degenerate SOMOs (singly occupied molecular orbitals) of a $[Ge_9R_3]^-$ moiety (Figure S2). The PIOs forming the "π-bonds" are mainly derived from the linear combinations of the tangential p orbitals of the Ge atoms localized on its open face (top layer) (Figure 2a). Thus, in order to maximize the "π-bonding" interaction between the two cages, the two Ge_9R_3 cages are observed in an eclipsed arrangement (here referring to the six cage Ge atoms from the two top layers) in compound **1**, rather than a staggered arrangement as in the $[Pd_2E_{18}]^{4-}$ cluster.[23,26] For comparison, we also carried out PIO analysis on the analogous borane compound $[B_{21}H_{18}]^-$, and significantly reduced PBIs were obtained, indicating the substantial difference between cluster **1** and its borane analog (Figure S3).

To further justify our argument, we performed DFT calculation on the hypothetical cluster $[Ge_{18}(SnMe_3)_6]^{2-}$ obtained by removal of the three Pd centers from **1′**.

DOI: 10.1021/acs.inorgchem.8b03640
Inorg. Chem. 2019, 58, 3473−3478

Calculation results suggest that the structure is still stable (Figure 2b). The PIO analysis has also been carried out on this hypothetical cluster, and it can be clearly seen that the two Ge_9R_3 cages are held together by a pair of "π-bonds" (Figure S4). Therefore, we are confident to believe that the cluster compound **1**, $[Pd_3Ge_{18}(Sn^iPr_3)_6]^{2-}$, should be understood as two $[Ge_9R_3]^-$ cages held together by a pair of remote "π-bonds", with three neutral Pd centers inserted in between, stabilizing the whole cluster. An orbital interaction diagram corresponding to our analysis can be found in Figure 3 (a more complete version is given in Figure S5).

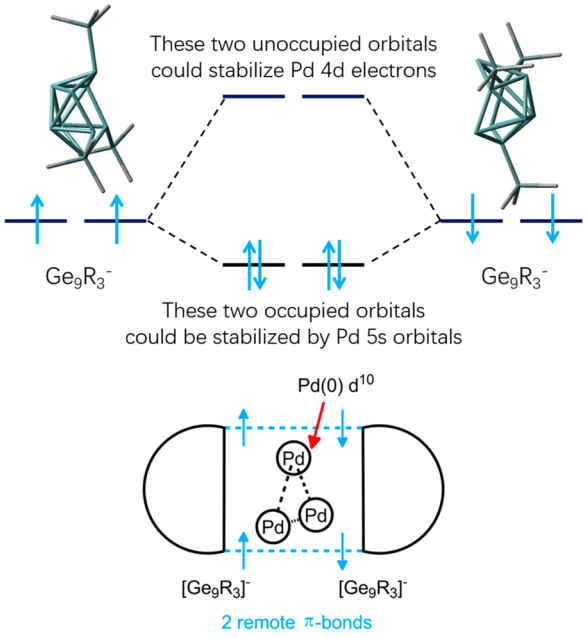

Figure 3. Proposed orbital interaction diagram for the cluster compound **1** and a Lewis-like schematic representation describing its electronic structure.

From the above analysis, we can see that the $Ge_9R_3^-$ cage formally adopts a triplet electronic configuration in cluster **1**, which is quite unexpected because isolated $Ge_9R_3^-$ clusters have been synthesized with a singlet ground state. The reason why we have to base our understanding of cluster **1** on a triplet $Ge_9R_3^-$ is far from trivial. To illustrate this point, we would like to take the cluster compound $[Pd(Ge_9R_3)_2]^{2-}$ as an example, in which there are two $Ge_9R_3^-$ cages coordinating to a single Pd center.[20] In this case, the $Ge_9R_3^-$ cages adopt a tricapped trigonal prismatic (TTP, D_{3h}) geometry as they usually do. Actually, the HOMO of $Ge_9R_3^-$ in the tricapped trigonal prismatic structure is a singly degenerate orbital of a_2 symmetry, while its LUMO and LUMO + 1 are degenerate and of e symmetry.[36,37] However, for a distorted TTP (C_{3v}) like the Ge_9R_3 cages present in cluster **1**, the a_2 orbital is pushed higher in orbital energy than the e orbital pair. Therefore, a triplet electronic configuration results. A schematic illustration of the argument given here is shown in Figure 4.

The interaction between the Pd_3-triangle and ligands is similar to the scenario in the previously reported complex $[Pd_3X_3(C_7H_7)_2]^-$, in which there is also a Pd_3-triangle sandwiched by two C_7H_7 ligands.[38] This complex is similar to the clusters **1** and **2** discussed here, in the sense that the two C_7H_7 ligands play a similar role as the two Ge_9R_3 cages in

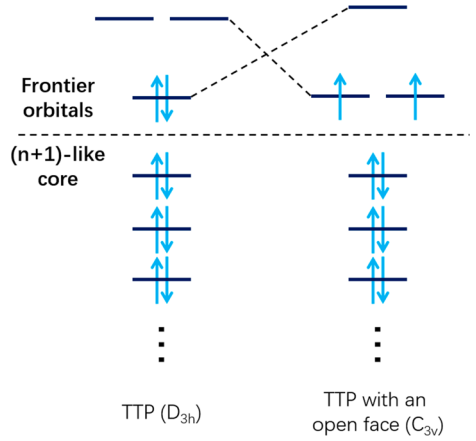

Figure 4. Schematic orbital diagram of $Ge_9R_3^-$ in two different geometries. The distorted TTP (C_{3v}) geometry represents the skeletal framework of the Ge_9R_3 fragments in cluster **1**.

clusters **1** and **2**, both stabilizing the neutral Pd_3-triangle via multiple donation and back-donation interactions. Nevertheless, the fact that the three Pd centers perfectly avoid the three Ge−Ge contacts across the two Ge_9 fragments also contributes to the overall stability of the whole cluster and makes this example rather unique.

After obtaining such a fragment-based description of the electronic structure of cluster compound **1**, it would be much easier to understand the interesting arrangement of the six substituents. Although the two Ge_9R_3 cages in **1** share a similar skeletal arrangement, the stannyl groups in one cage are bonded to the three Ge atoms on the top layer, while in the other one they are bonded to the three Ge atoms in the middle layer. While syntheses of the middle-layer-decorated cage have been commonly reported in the literature,[11−15,18−20] why substituents would like to move to the open face in only one cage remains a question.

To answer this question, we performed single-point energy calculations on the two differently decorated $[Ge_9(SnMe_3)_3]$ cages with various charge assignments, on the basis of the distorted TTP fragments from the optimized cluster (**1**). The calculation results (Table 1) show that the relatively electron-

Table 1. Relative Single-Point Energies of Ge_9R_3 (R = $SnMe_3$) Cages with Different Decoration Sites and Different Charges

ΔE (kcal/mol)	$[Ge_9R_3]^+$	$[Ge_9R_3]^{-b}$	$[Ge_9R_3]^{3-}$
m-isomer[a]	0.0	0.0	42.2
t-isomer[a]	25.8	5.4	0.0

[a] *m*/*t*-isomer denotes the substitution sites on the Ge_9 cage. *m* stands for substitution on the middle layer and *t* stands for that on the top layer (see Figure 1d). [b] The $Ge_9R_3^-$ moiety is calculated with a triplet configuration.

deficient species $[Ge_9R_3]^+$ favors the middle-layer-decorated structure, while the relatively electron-rich species $[Ge_9R_3]^{3-}$ favors the open-face-decorated one. The intermediate one $[Ge_9R_3]^-$ shows only very slight preference to the middle layer-decorated structure. The different preference should be attributed to the fact that additional electrons in the degenerate HOMOs of $[Ge_9R_3]^{3-}$ are localized on its open face (top layer) and can be better stabilized by the substituents which are formally considered as cationic. We therefore come

DOI: 10.1021/acs.inorgchem.8b03640
Inorg. Chem. 2019, 58, 3473−3478

to a conclusion that, although isolated Ge_9R_3 cages have only been observed in the form of *m*-$[Ge_9R_3]^-$,[18,19] the open-face-decorated cage becomes more stable when the two $[Ge_9R_3]^-$ cages form a pair of π-bonds (in compound **1**).

Keeping this idea in mind, we then optimized two other isomers of compound **1′** with stannyl substituents at different positions (all of the six substituents occupy the middle-layer sites or the top-layer sites on the two cages). Results show that the asymmetric arrangement (the experimentally observed one), in which three substituents occupy the middle-layer sites on one cage and the remaining three substituents occupy the top-layer sites on the other cage, is indeed more stable than the isomer in which all substituents are on the middle layer, in agreement with the published data done by the experimental group,[30] which we attribute to the better stabilization of the additional electrons used for the "remote π-bonds". However, the isomer with all substituents attached on the open face (top-layer sites) has the highest energy among the three isomers. This should be attributed to strong steric repulsion among the six substituents. To justify this argument, we also optimized the three isomers with all stannyl groups being replaced with hydrogens. The calculation results now agree with our conjecture that, the more substituents attached on the open face, the more stable is the isomer (Table 2). We hence conclude that the electronic factor prefers more substituents attached on the open face, while the steric factor prefers middle-layer decoration. As pointed out in ref 30, the silyl groups (present in cluster **2**) are closer to the skeleton (due to smaller size of Si versus Sn) and hence have larger steric repulsion with each other. The balance between electronic factor and steric factor eventually leads to the different substitution patterns observed in clusters **1** and **2**, consistent with the conclusion made by the experimental group.[28]

Table 2. Relative Electronic and Free Energies of Three Isomers of $[Pd_3Ge_{18}R_6]^{2+}$ with R = $SnMe_3$, H

ΔG (ΔE) (kcal/mol)	$[Pd_3Ge_{18}(SnMe_3)_6]^{2-}$	$[Pd_3Ge_{18}H_6]^{2-}$
mm-isomer[a]	9.8 (8.9)	17.7 (19.8)
tm-isomer[a]	0.0 (0.0)	9.0 (10.4)
tt-isomer[a]	26.7 (18.8)	0.0 (0.0)

[a]*mm*/*tm*/*tt*-isomer denotes the substitution sites on the two Ge_9 cages. *m* stands for substitution on the middle layer and *t* stands for that on the top layer.

In conclusion, with the aid of PIO analysis, we found that the cluster compound $[Pd_3Ge_{18}R_6]^{2-}$ (R = Sn^iPr_3, (**1**); R = Si^iPr_3, (**2**)) has a pair of remote "π-bonds" that hold the two $[Ge_9R_3]^-$ cages together, which explains the eclipsed arrangement of these two Ge_9 cages. The orbitals that each cage utilizes to form the remote bonds are consistent with our established frontier orbitals for $[E_9]^{2-}$ and $[M@E_9]^{2-}$ (M = d^{10} metal centers) fragments in previous works,[31,37] and we have demonstrated how these frontier orbitals behave when the Ge_9 cage adopts different geometries. The Pd centers merely play a role in stabilizing the overall cluster through donor−acceptor interactions with these frontier orbitals of cages (Figures S1 and S5). To better stabilize the remote "π-bonds", substituents tend to locate on the top layer of each Ge_9R_3 cage, i.e., the sites on the open face that the cage utilizes to form bonds with another cage. The different substitution patterns result from the balance between electronic preference (for cage atoms in different layers) and steric repulsion (among the substituents). We have demonstrated the power of PIO analysis in helping us analyze the orbital interaction between fragments in the title cluster compounds in a straightforward manner. We will continue to apply PIO analysis to other cluster compounds to unravel the mystery in their bonding pictures.

COMPUTATIONAL DETAILS

All calculations are performed with Gaussian 09 program.[39] All of the structures are optimized using PBE0 functional.[40] Def2-TZVP basis set is used for all atoms along with associated pseudopotentials,[41] except carbon and hydrogen atoms in ^{i}Pr-substituted clusters **1** and **2**, for which a standard 6-31G* basis set is used.[42] Vibrational analyses have been performed to ensure all the structures have no imaginary frequencies. Natural population analysis (NPA) is performed by NBO6.0 software.[35,43] Principal interacting orbital (PIO) analysis is carried out using the publicly available code on GitHub.[31] Spin natural orbitals (SNOs) are calculated via in-house code.[44] All orbital plots have an isolvalue of 0.05 unless particularly specified. To verify the relativistic effect does not significantly affect calculation results, we have also performed single-point calculations incorporating DKH2 Hamiltonian[45,46] on the optimized structures of different isomers of cluster **1′**. The results show that regular DFT calculations produce the same order of relative energies as all-electron DKH2 calculations (Table S1). For DKH2 calculations, an all-electron x2c-TZVP basis set is used for Pd, Ge, and Sn atoms and a x2c-SVP basis set, for C and H atoms.[47]

ASSOCIATED CONTENT

Supporting Information

The Supporting Information is available free of charge on the ACS Publications website at DOI: 10.1021/acs.inorgchem.8b03640.

Comparison of results using non-relativistic DFT and all-electron DKH2 calculations, MO and SNO analyses on the Ge_9R_3 fragment, additional PIO analyses on cluster **1'** and the hypothetical cluster $[Ge_{18}R_6]^{2-}$, and supplementary schematic orbital diagram for cluster **1** (PDF)

Cartesian coordinates of all optimized structures (XYZ)

AUTHOR INFORMATION

Corresponding Authors

*E-mail: fksheong@connect.ust.hk (F.K.S.).
*E-mail: chzlin@ust.hk (Z.L.).

ORCID

Zhenyang Lin: 0000-0003-4104-8767

Funding

This work was supported by the Research Grant Council of Hong Kong (HKUST 16304017).

Notes

The authors declare no competing financial interest.

REFERENCES

(1) Schnepf, A. Novel Compounds of Elements of Group 14: Ligand-Stabilized Clusters with "Naked" Atoms. *Angew. Chem., Int. Ed.* **2004**, *43* (6), 664−666.

(2) Schnepf, A. Metalloid Cluster Compounds of Germanium: A Novel Class of Germanium Cluster Compounds of Formulae Ge_nR_m (n > m). *Coord. Chem. Rev.* **2006**, *250* (21), 2758−2770.

(3) Schnepf, A. Metalloid Group 14 Cluster Compounds: An Introduction and Perspectives to This Novel Group of Cluster Compounds. *Chem. Soc. Rev.* **2007**, *36* (5), 745−758.

(4) Scharfe, S.; Kraus, F.; Stegmaier, S.; Schier, A.; Fässler, T. F. Zintl Ions, Cage Compounds, and Intermetalloid Clusters of Group

DOI: 10.1021/acs.inorgchem.8b03640
Inorg. Chem. 2019, 58, 3473−3478

14 and Group 15 Elements. *Angew. Chem., Int. Ed.* **2011**, *50* (16), 3630−3670.
(5) Mayer, K.; Weßing, J.; Fässler, T. F.; Fischer, R. A. Intermetalloid Clusters: Molecules and Solids in a Dialogue. *Angew. Chem., Int. Ed.* **2018**, *57* (44), 14372.
(6) Prabusankar, G.; Kempter, A.; Gemel, C.; Schröter, M.-K.; Fischer, R. A. $[Sn_{17}\{GaCl(ddp)\}_4]$: A High-Nuclearity Metalloid Tin Cluster Trapped by Electrophilic Gallium Ligands. *Angew. Chem., Int. Ed.* **2008**, *47* (38), 7234−7237.
(7) Schenk, C.; Henke, F.; Schnepf, A. $[Ge_{12}\{FeCp(CO)_2\}_8\{FeCp(CO)\}_2]$: A Ge_{12} Core Resembles the Arrangement of the High-Pressure Modification Germanium (II). *Angew. Chem., Int. Ed.* **2013**, *52* (6), 1834−1838.
(8) Schnepf, A.; Schenk, C. $Na_6[Ge_{10}\{Fe(CO)_4\}_8]\cdot 18$ THF: A Centaur Polyhedron of Germanium Atoms. *Angew. Chem., Int. Ed.* **2006**, *45* (32), 5373−5376.
(9) Brynda, M.; Herber, R.; Hitchcock, P. B.; Lappert, M. F.; Nowik, I.; Power, P. P.; Protchenko, A. V.; Růžička, A.; Steiner, J. Higher-Nuclearity Group 14 Metalloid Clusters: $[Sn_9\{Sn(NRR')\}_6]$. *Angew. Chem., Int. Ed.* **2006**, *45* (26), 4333−4337.
(10) Schnepf, A. Metalloid Cluster Compounds of Germanium: Synthesis − Properties − Subsequent Reactions. *Eur. J. Inorg. Chem.* **2008**, *2008* (7), 1007−1018.
(11) Kysliak, O.; Schrenk, C.; Schnepf, A. $\{Ge_9[Si(SiMe_3)_2(SiPh_3)]_3\}^-$: Ligand Modification in Metalloid Germanium Cluster Chemistry. *Inorg. Chem.* **2015**, *54* (14), 7083−7088.
(12) Schenk, C.; Schnepf, A. $[AuGe_{18}\{Si(SiMe_3)_3\}_6]^-$: A Soluble Au−Ge Cluster on the Way to a Molecular Cable? *Angew. Chem., Int. Ed.* **2007**, *46* (28), 5314−5316.
(13) Henke, F.; Schenk, C.; Schnepf, A. $[Si(SiMe_3)_3]_6Ge_{18}M$ (M = Zn, Cd, Hg): Neutral Metalloid Cluster Compounds of Germanium as Highly Soluble Building Blocks for Supramolecular Chemistry. *Dalton Trans.* **2009**, *0* (42), 9141−9145.
(14) Schenk, C.; Henke, F.; Santiso-Quiñones, G.; Krossing, I.; Schnepf, A. $[Si(SiMe_3)_3]_6Ge_{18}M$ (M = Cu, Ag, Au): Metalloid Cluster Compounds as Unusual Building Blocks for a Supramolecular Chemistry. *Dalton Trans.* **2008**, *0* (33), 4436−4441.
(15) Kysliak, O.; Schrenk, C.; Schnepf, A. The Largest Metalloid Group 14 Cluster, $Ge_{18}[Si(SiMe_3)_3]_6$: An Intermediate on the Way to Elemental Germanium. *Angew. Chem., Int. Ed.* **2016**, *55* (9), 3216−3219.
(16) Schenk, C.; Schnepf, A. $\{Ge_9R_3Cr(CO)_5\}^-$ and $\{Ge_9R_3Cr(CO)_3\}^-$: A Metalloid Cluster $(Ge_9R_3^-)$ as a Flexible Ligand in Coordination Chemistry [R = $Si(SiMe_3)_3$]. *Chem. Commun.* **2009**, *0* (22), 3208−3210.
(17) Henke, F.; Schenk, C.; Schnepf, A. $[Si(SiMe_3)_3]_3Ge_9M(CO)_3^-$ (M = Cr, Mo, W): Coordination Chemistry with Metalloid Clusters. *Dalton Trans.* **2011**, *40* (25), 6704−6710.
(18) Schnepf, A. $[Ge_9\{Si(SiMe_3)_3\}_3]^-$: A Soluble Polyhedral Ge_9 Cluster Stabilized by Only Three Silyl Ligands. *Angew. Chem., Int. Ed.* **2003**, *42* (23), 2624−2625.
(19) Li, F.; Sevov, S. C. Rational Synthesis of $[Ge_9\{Si(SiMe_3)_3\}_3]^-$ from Its Parent Zintl Ion Ge_9^{4-}. *Inorg. Chem.* **2012**, *51* (4), 2706−2708.
(20) Li, F.; Sevov, S. C. Coordination of Tri-Substituted Nona−Germanium Clusters to Cu(I) and Pd(0). *Inorg. Chem.* **2015**, *54* (16), 8121−8125.
(21) Li, F.; Sevov, S. C. Synthesis, Structures, and Solution Dynamics of Tetrasubstituted Nine-Atom Germanium Deltahedral Clusters. *J. Am. Chem. Soc.* **2014**, *136* (34), 12056−12063.
(22) Li, F.; Muñoz-Castro, A.; Sevov, S. C. $[Ge_9\{Si(SiMe_3)_3\}_3\{SnPh_3\}]$: A Tetrasubstituted and Neutral Deltahedral Nine-Atom Cluster. *Angew. Chem., Int. Ed.* **2012**, *51* (34), 8581−8584.
(23) Goicoechea, J. M.; Sevov, S. C. $[(Pd{-}Pd)@Ge_{18}]^{4+}$: A Palladium Dimer Inside the Largest Single-Cage Deltahedron. *J. Am. Chem. Soc.* **2005**, *127* (21), 7676−7677.
(24) Schrenk, C.; Winter, F.; Pöttgen, R.; Schnepf, A. $\{Sn_9[Si(SiMe_3)_3]_2\}^{2-}$: A Metalloid Tin Cluster Compound With a Sn_9 Core of Oxidation State Zero. *Inorg. Chem.* **2012**, *51* (15), 8583−8588.
(25) Li, F.; Muñoz-Castro, A.; Sevov, S. C. $[(Me_3Si)Si]_3EtGe_9Pd(PPh_3)$, a Pentafunctionalized Deltahedral Zintl Cluster: Synthesis, Structure, and Solution Dynamics. *Angew. Chem., Int. Ed.* **2016**, *55* (30), 8630−8633.
(26) Sun, Z.-M.; Xiao, H.; Li, J.; Wang, L.-S. $Pd_2@Sn_{18}^{4-}$: Fusion of Two Endohedral Stannaspherenes. *J. Am. Chem. Soc.* **2007**, *129* (31), 9560−9561.
(27) Belin, C. H. E.; Corbett, J. D.; Cisar, A. Homopolyatomic Anions and Configurational Questions. Synthesis and Structure of the Nonagermanide(2-) and Nonagermanide(4-) Ions, Ge_9^{2-} and Ge_9^{4-}. *J. Am. Chem. Soc.* **1977**, *99* (22), 7163−7169.
(28) Mingos, D. M. P.; Wales, D. J. *Introduction to Cluster Chemistry*; Prentice-Hall: Englewood Cliffs, NJ, 1990.
(29) Perla, L. G.; Sevov, S. C. A Stannyl-Decorated Zintl Ion $[Ge_{18}Pd_3(Sn^iPr_3)_6]^{2-}$: Twinned Icosahedron with a Common Pd_3-Face or 18-Vertex Hypho-Deltahedron with a Pd_3-Triangle Inside. *J. Am. Chem. Soc.* **2016**, *138* (31), 9795−9798.
(30) Perla, L. G.; Muñoz-Castro, A.; Sevov, S. C. Eclipsed- and Staggered-$[Ge_{18}Pd_3\{E^iPr_3\}_6]^{2-}$ (E = Si, Sn): Positional Isomerism in Deltahedral Zintl Clusters. *J. Am. Chem. Soc.* **2017**, *139* (42), 15176−15181.
(31) Zhang, J.-X.; Sheong, F. K.; Lin, Z. Unravelling Chemical Interactions with Principal Interacting Orbital Analysis. *Chem. - Eur. J.* **2018**, *24* (38), 9639−9650.
(32) Bernhardt, E.; Brauer, D. J.; Finze, M.; Willner, H. *closo*-$[B_{21}H_{18}]^-$: A Face-Fused Diicosahedral Borate Ion. *Angew. Chem., Int. Ed.* **2007**, *46* (16), 2927−2930.
(33) Balakrishnarajan, M. M.; Jemmis, E. D. Electronic Requirements of Polycondensed Polyhedral Boranes. *J. Am. Chem. Soc.* **2000**, *122* (18), 4516−4517.
(34) Jemmis, E. D.; Balakrishnarajan, M. M.; Pancharatna, P. D. A Unifying Electron-Counting Rule for Macropolyhedral Boranes, Metallaboranes, and Metallocenes. *J. Am. Chem. Soc.* **2001**, *123* (18), 4313−4323.
(35) Reed, A. E.; Weinstock, R. B.; Weinhold, F. Natural Population Analysis. *J. Chem. Phys.* **1985**, *83* (2), 735−746.
(36) Johnston, R. L.; Mingos, D. M. P. Molecular Orbital Calculations Relevant to the Hyper-Closo vs. Iso-Closo Controversy in Metallaboranes. *Inorg. Chem.* **1986**, *25* (18), 3321−3323.
(37) Sheong, F. K.; Chen, W.-J.; Zhang, J.-X.; Li, Y.; Lin, Z. Structure and Bonding of $[Pd_2Sn_{18}]^{4-}$: An Interesting Example of the Mutual Delocalisation Phenomenon. *Dalton Trans.* **2017**, *46* (7), 2214−2219.
(38) Muñoz-Castro, A.; Arratia-Pérez, R. Electronic Delocalization, Energetics, and Optical Properties of Tripalladium Ditropylium Halides, $[Pd_3(C_7H_7)_2X_3]^{1-}$ (X = Cl^-, Br^-, and I^-). *J. Phys. Chem. A* **2010**, *114* (15), 5217−5221.
(39) Frisch, M. J.; Trucks, G. W.; Schlegel, H. B.; Scuseria, G. E.; Robb, M. A.; Cheeseman, J. R.; Scalmani, G.; Barone, V.; Mennucci, B.; Petersson, G. A.; Nakatsuji, H.; Caricato, M.; Li, X.; Hratchian, H. P.; Izmaylov, A. F.; Bloino, J.; Zheng, G.; Sonnenberg, J. L.; Hada, M.; Ehara, M.; Toyota, K.; Fukuda, R.; Hasegawa, J.; Ishida, M.; Nakajima, T.; Honda, Y.; Kitao, O.; Nakai, H.; Vreven, T.; Montgomery, J. A., Jr.; Peralta, J. E.; Ogliaro, F.; Bearpark, M.; Heyd, J. J.; Brothers, E.; Kudin, K. N.; Staroverov, V. N.; Kobayashi, R.; Normand, J.; Raghavachari, K.; Rendell, A.; Burant, J. C.; Iyengar, S. S.; Tomasi, J.; Cossi, M.; Rega, N.; Millam, J. M.; Klene, M.; Knox, J. E.; Cross, J. B.; Bakken, V.; Adamo, C.; Jaramillo, J.; Gomperts, R.; Stratmann, R. E.; Yazyev, O.; Austin, A. J.; Cammi, R.; Pomelli, C.; Ochterski, J. W.; Martin, R. L.; Morokuma, K.; Zakrzewski, V. G.; Voth, G. A.; Salvador, P.; Dannenberg, J. J.; Dapprich, S.; Daniels, A. D.; Farkas, Ö.; Foresman, J. B.; Ortiz, J. V.; Cioslowski, J.; Fox, D. J. *Gaussian 09*, Revision D.01; Gaussian Inc.: Wallingford, CT, 2009.
(40) Adamo, C.; Barone, V. Toward Reliable Density Functional Methods without Adjustable Parameters: The PBE0 Model. *J. Chem. Phys.* **1999**, *110* (13), 6158−6170.

DOI: 10.1021/acs.inorgchem.8b03640
Inorg. Chem. 2019, 58, 3473−3478

(41) Weigend, F.; Ahlrichs, R. Balanced Basis Sets of Split Valence, Triple Zeta Valence and Quadruple Zeta Valence Quality for H to Rn: Design and Assessment of Accuracy. *Phys. Chem. Chem. Phys.* **2005**, *7* (18), 3297−3305.
(42) Hariharan, P. C.; Pople, J. A. The Influence of Polarization Functions on Molecular Orbital Hydrogenation Energies. *Theor. Chim. Acta* **1973**, *28* (3), 213−222.
(43) Glendening, E. D.; Landis, C. R.; Weinhold, F. NBO 6.0: Natural Bond Orbital Analysis Program. *J. Comput. Chem.* **2013**, *34* (16), 1429−1437.
(44) Sheong, F. K.; Zhang, J.-X.; Lin, Z. Revitalizing Spin Natural Orbital Analysis: Electronic Structures of Mixed-Valence Compounds, Singlet Biradicals, and Antiferromagnetically Coupled Systems. *J. Comput. Chem.* **2019**, DOI: 10.1002/jcc.25762.
(45) Douglas, M.; Kroll, N. M. Quantum Electrodynamical Corrections to the Fine Structure of Helium. *Ann. Phys.* **1974**, *82* (1), 89−155.
(46) Jansen, G.; Hess, B. A. Revision of the Douglas-Kroll Transformation. *Phys. Rev. A: At., Mol., Opt. Phys.* **1989**, *39* (11), 6016−6017.
(47) Pollak, P.; Weigend, F. Segmented Contracted Error-Consistent Basis Sets of Double- and Triple-ζ Valence Quality for One- and Two-Component Relativistic All-Electron Calculations. *J. Chem. Theory Comput.* **2017**, *13* (8), 3696−3705.

DOI: 10.1021/acs.inorgchem.8b03640
Inorg. Chem. 2019, 58, 3473−3478